membranes

MDPI

Article

Formic Acid-Electrospun Polyhydroxybutyrate Fibrous Membranes Loaded with In Situ-Generated Organo-Titania Nanophase: Preparation and Photocatalytic Activity

Hristo Penchev [1,*], Eman A. Ali [2], Katerina Zaharieva [3,*], Ahmed E. Abdelhamid [2], Filip Ublekov [1], Silvia Dimova [1], Dessislava Budurova [1], Ognyan Dimitrov [4], Maria Shipochka [5], Ahmed A. El-Sayed [6] and Ahmed M. Khalil [6,*]

1 Institute of Polymers, Bulgarian Academy of Sciences, "Akad. G. Bonchev" St., Block 103A, 1113 Sofia, Bulgaria; ublekov.philip@gmail.com (F.U.); dimova@polymer.bas.bg (S.D.); dbudurova@polymer.bas.bg (D.B.)
2 Polymers and Pigments Department, National Research Centre, El-Buhouth St., Giza 12622, Egypt; eman.abobakr@outlook.com (E.A.A.); ahmednrc10@gmail.com (A.E.A.)
3 Institute of Mineralogy and Crystallography "Acad. I. Kostov", Bulgarian Academy of Sciences, Acad. G. Bonchev St., Block 107, 1113 Sofia, Bulgaria
4 Institute of Electrochemistry and Energy Systems "Acad. Evgeni Budevski", Bulgarian Academy of Sciences, Acad. G. Bonchev St., Block 10, 1113 Sofia, Bulgaria; ognian.dimitrov@iees.bas.bg
5 Institute of General and Inorganic Chemistry, Bulgarian Academy of Sciences, "Acad. G. Bonchev" St., Bl. 11, 1113 Sofia, Bulgaria; shipochka@svr.igic.bas.bg
6 Photochemistry Department, National Research Centre, El-Buhouth St., Dokki, Giza 12622, Egypt; ahmedcheme4@yahoo.com
* Correspondence: hpen4ev@gmail.com (H.P.); zaharieva@imc.bas.bg (K.Z.); akhalil75@yahoo.com (A.M.K.)

Abstract

Biodegradable polyhydroxybutyrate, an electrospinnable polyester derived from microbial sources, was incorporated with an in situ-synthesized titania-formate nanophase at various concentrations. Formic acid was used as both a reactive solvent for the sol–gel precursor and a spinning solvent for PHB. This work aims to investigate the photocatalytic activity of the fabricated electrospun mats towards degrading methylene blue (MB), a model dye pollutant, in contaminated water. The tested mats were soaked in an aqueous ammonia solution to enhance the catalytic activity of the organo-titanium nanophase through this basic treatment. The morphology, structure, and thermal stability of the electrospun mats were evaluated through SEM, ATR FT-IR, TG, XPS, and WAXD analyses. The water contact angle measurements indicated that the amorphous organo-titania phase influences the surface hydrophobicity of the PHB mat (CA = 109°), with a contact angle reduction down to 86° for the PHB/TiFA 10 NH_3 mat. Increasing the organo-titania NP loading resulted in a proportional decrease in the water contact angle, indicating a slight enhancement in the hydrophilicity of the composite. The MB dye photodegradation kinetics using the tested composite nanofibrous substrates loaded with the in situ-generated organo-titania nanophase were evaluated under daylight irradiation, showing remarkable photodegradation results. The nanofiber mats (2.5 mg immersed in 10 mL of dye solution) reached 94.2 to 78% for the MB dye, with the concentration ranging from 5 to 25 ppm, respectively.

Keywords: polyhydroxybutyrate; titania; mats; photocatalyst; methylene blue dye; degradation

Check for updates

Academic Editors: Qieyuan Gao and Shuai Guo

Received: 16 October 2026
Revised: 22 November 2026
Accepted: 23 November 2026
Published: 27 November 2026

Copyright: © 2026 by the authors. Licensee MDPI, Basel, Switzerland. This article is an open access article distributed under the terms and conditions of the Creative Commons Attribution (CC BY) license.

1. Introduction

Photocatalysis has been shown to be an inexpensive and effective method for treating a wide range of organic and inorganic pollutants in both water and air [1]. Nanocrystalline semiconductors, mainly TiO_2, are widely studied in photocatalytic reactions because of their chemical stability, low toxicity, low cost, and commercial availability [2,3].

The importance of the immobilization of the catalysts in a polymer matrix or on a sustainable support with a highly developed surface for applications in photocatalysis has been growing in recent years, mainly due to their ease of removal from the aqueous medium and reusability [4,5].

According to Singh et al. [6], the synthetic and bio-based polymers, e.g., polyhydroxyalkanoates (PHAs), represent a viable alternative to be used as a support for inorganic photocatalysts, e.g., ZnO- and TiO_2-based metal-oxide NPs incorporated into polymer hybrids and composites. Their important intrinsic properties can be summarized as: (i) being chemically inert to the medium; (ii) hydrophilic–hydrophobic balance allows them to retain the pollutants on their surface, leading to increased efficiency both in the adsorption and perhaps in the following oxidation (oxidative degradation); (iii) are accessible and can be found in abundance; (iv) low density (float in the aqueous medium), being easily removable and disposable. Titanium dioxide in the form of the anatase phase is a widely available and chemically robust semiconductor with a long history of research in the area of photocatalysts in particular. However, its practical application is limited by a wide bandgap (~3.2 eV) and rapid electron–hole recombination, restricting its photocatalytic activity to the UV region. In recent years, new photocatalyst research has emerged from studying the so-called Magnéli-phase non-stoichiometric titania suboxides (Ti_nO_{2n-1}), or "black titania", which exhibit a reduced bandgap (~1.5 eV), the presence of mixed Ti^{3+}/Ti^{4+} valence, and significantly enhanced solar absorption (83%), making it a promising material for next-generation energy and environmental applications [7]. Campostrini et al. employed the sol–gel method using a titanium(IV) isopropoxide precursor with the use of formic acid as a chelating agent, which allows the easy preparation of amorphous TiO_2 gels with a high specific surface area, subsequently yielding polycrystalline anatase TiO_2 powders by pyrolysis at temperatures close to 420 °C [8]. In addition, the uniform distribution and immobilization of titania NPs within different polymer matrices as a photocatalyst may lead to the optimization of light absorption [6].

Polyhydroxybutyrate (PHB) is a microbial bioprocessed polyester belonging to the PHA family. This biocompatible, environmentally friendly, and non-toxic polymer is biosynthesized and accumulated by a number of specialized bacterial strains [9,10]. Several decades of research dedicated to the development of the electrospinning technique have established it as a feasible approach for the preparation of high surface-area-to-volume micro- and nanofibrous nonwoven mats from a great variety of polymers and polymer-inorganic composite materials [11]. The electrospinning of highly crystalline and inherently brittle PHB mats from traditional halogenated hydrocarbon solvents (e.g., chloroform or dichloromethane) is still a significant drawback for their practical use. In this regard, the addition of suitable amorphizing inorganic fillers, such as natural or organo-modified montmorillonites, and/or the use of polar and highly volatile organic solvents, e.g., 1,1,1,3,3,3-hexafluoro-2-propanol or green-chemistry-based formic acid, are highly appreciated [12–17].

Korina et al. prepared magnetic PHB-based core–shell fibers decorated with TiO_2 as effective recyclable hybrid materials for the purification of water from organic pollutants, such as methylene blue (MB) dye, under UV light [18]. Nanostructured fibrous materials of PHB, TiO_2-in-PHB, and TiO_2-on-PHB were prepared by electrospinning, either alone or in

conjunction with electrospraying, by Spasova et al. [19]; the obtained composite materials demonstrated considerable antifungal activity against *P. chlamydospora*.

Based on our previous research and the accumulated knowledge on formic acid-electrospun PHB-based composite fibers, the aim of the present study is to prepare novel nanocomposite PHB mats with an incorporated mixed-valence Ti^{3+}/Ti^{4+} amorphous organo-titanate nanophase via a single-step green electrospinning approach with the use of formic acid—acting simultaneously as a reactive sol–gel precursor chelator and volatile spinning solvent. Furthermore, we investigated the photocatalytic activity of the newly prepared composite nanofibrous membranes under UV irradiation and daylight towards MB as a model pollutant dye.

2. Materials and Methods

Materials

Poly(3-hydroxybutyrate) powder from a bacterial origin with an average molecular mass of 230,000 g·mol^{-1}, kindly supplied by Dr. Urs Hanggi (Biomer, Krailling, Germany), and titanium(IV) n-butoxide ($Ti(OBu)_4$) (99+%, Alfa Aesar, Waltham, MA, USA) were used as the polymer matrix and the titania precursor, respectively. Formic acid (Merck, 99%, Darmstadt, Germany) was used as the solvent for both the polymer and the in situ sol–gel reaction. Methylene blue (MB) is a product of LOBACHEMIE, Mumbai, India. All chemicals were used as received without further purification.

2.1. Preparation of Polyhydroxybutyrate Electrospun Fibrous Membranes Loaded with Amorphous TiO_2 FA Nanophase

Synthesis of polymeric titanium alkoxide-formate: TiFA nanoparticles

Stable colloidal dispersions of polyalkoxide TiFA nanoparticles were synthesized via a controlled sol–gel pathway under highly acidic conditions. In a typical procedure, one milliliter of $Ti(OBu)_4$ precursor was dissolved in 50 g of pure formic acid (HCOOH). To ensure complete homogenization and initiate the polycondensation sol–gel reaction, the mixture was subjected to intense ultrasonic irradiation for 2 min. The formation of a characteristic white opalescent suspension containing TiFA nanoparticles was observed within approximately ten minutes, with subsequent magnetic stirring carried out at 600 rpm. The resulting nanoparticles were isolated by filtration with a 0.1-micron PTFE filter and purified by two consecutive washing steps, each using 10 mL of 96% ethanol. The resultant wet cake of coagulated particles was further vacuum-dried at 90 °C overnight. The resulting dry powder yield of TiFA was 0.470 g.

Electrospinning of composite PHB-TiFA nanofibers

In order to fabricate composite electrospun PHB fibers with two TiFA loadings (5 and 10 wt.% theoretical TiO_2 content), 0.5 g of PHB powder was first dispersed under vigorous stirring at room temperature into some pre-formed TiFA nanoparticle dispersions (prepared from the reaction of 0.1 and 0.2 g of $Ti(OBu)_4$ in 9.5 g of formic acid, respectively). Subsequently, the wetted PHB was dissolved under continuous stirring at 70 °C, resulting in a homogeneous composite polymer dope solution with a 5 wt.% concentration of dissolved PHB. The nonwoven fibrous membranes were fabricated using a custom-engineered laboratory electrospinning platform equipped with a standard single-needle stainless-steel spinneret (inner diameter: 0.8 mm, 21 G) connected to a high-voltage power supply. The fibers were deposited onto a flat, grounded aluminum plate collector (15 × 15 cm). All experiments were carried out inside a climate-controlled enclosure maintained at a constant ambient temperature of 23 ± 2 °C and a relative humidity of 65 ± 5%. The electrospinning process was carried out under the following optimized parameters: an applied voltage of

18 kV; a tip-to-collector distance of 22 cm; and a solution flow rate maintained between 1 mL/h and 3 mL/h. For the neat 5 wt.% PHB-0 solution in FA, a constant flow rate of 1 mL/h was maintained, demonstrating good spinnability. For the PHB/TiFA composite solution, the electrospinning process was initiated at a feeding rate of 3 mL/h and subsequently adjusted to 2 mL/h to optimize fiber formation and deposition. The electrospinning deposition time was 1 h in all experiments, resulting in dense, self-supporting nanofibrous membranes; these were peeled off from the aluminum plate collector after pre-wetting with 96% ethanol and further vacuum-dried at 50 °C overnight.

Water–ammonia treatment of the PHB-TiFA fibrous membranes

Part of the obtained electrospun composite PHB mats containing TiFA NPs was subjected to water–ammonia solution treatment and subsequent heat treatment. First, 50 mL of concentrated 25 wt. % ammonia solution was diluted with 450 mL of deionized water. Preliminary cut 10 × 10 cm PHB/TiFA 5 and PHB/TiFA 10 fibrous membranes were immersed overnight in the resultant 2.5 wt. % water–ammonia solution bath, after which they were rinsed with deionized water and thermally treated at 150 °C in a vacuum furnace for another twelve hours.

2.2. Physico-Chemical Characterization of Prepared Polyhydroxybutyrate Electrospun Fibrous Membranes Loaded with Titania

The X-ray photoelectron spectroscopy (XPS) measurements were performed in a VG ESCALAB II electron spectrometer (VG Scientific, Birches Industrial Estate, Sussex, UK) using AlKα radiation, with an energy of 1486.6 eV. The binding energies were determined with an accuracy of ±0.1 eV, utilizing the C1s line at 285.0 eV (from adventitious carbon) as a reference. The chemical composition of the films was investigated on the basis of the areas and binding energies of the C1s, O1s, Ti2p, and N1s photoelectron peaks (after linear subtraction of the background) and Scofield's photoionization cross-sections. The surface morphology of the samples was studied with scanning electron microscopy (SEM) using a Zeiss Evo 10 microscope (Carl Zeiss Microscopy, Oberkochen, Germany). The photographs were taken in the secondary-electron and backscattered-electron modes, with an accelerating voltage in the range of 2–25 keV and no conductive coating on the samples. The chemical composition of the surface was investigated with an electron-dispersive spectroscopy (EDS) probe—Oxford Ultim Max 40 (Oxford Instruments, Abingdon, United Kingdom). The results were compiled with AZtec software (version 6.1 HF4). The statistical measurements of the PHB electrospun fibrous membranes were performed with Image J 1.53t software. The statistical measurements were performed on the basis of 100 individual fibers. TEM analyses were carried out on an HR STEM JEOL JEM 2100 (JEOL Ltd., Tokyo, Japan). Thermogravimetric analyses were performed in an argon atmosphere on a TGA-4000 Perkin Elmer instrument (PerkinElmer, Inc., Shelton, CT, USA, temperature range of 40–800 °C, 10 °C/min). Wide-angle X-ray diffraction (WAXD) scans were obtained on a Bruker D8 Advance ECO diffractometer (Bruker Corporation, Billerica, MA, USA) in reflection mode over the 2θ range of 5–60◦. The ATR FT-IR analyses were performed on an IRAffinity-1 Shimadzu apparatus (Shimadzu Corporation, Kyoto, Japan) in the range of 400–4000 cm^{-1}. The contact angle values were recorded with a camera attached to a computer. Deionized water droplets (5 µL) were transferred to the surface of the membrane at 25 °C to explore the hydrophilicity of the membranes. Each sample was tested 3 times for 5 s, and the average values were calculated and displayed in the graph with error bars.

2.3. Photocatalytic Study of Synthesized Polyhydroxybutyrate Electrospun Fibrous Membranes Loaded with Titania for Degradation of Methylene Blue Dye

The assessment of MB dye degradation was performed by testing different samples, PHB/TiFA 5, PHB/TiFA 5 NH_3, PHB/TiFA 10, and PHB/TiFA 10 NH_3, over a duration of 60 min. The best-performing sample was further evaluated by examining the effects of varying contact times (60, 120, 180, 240, and 300 min) and different dye concentrations (5, 10, 15, 20, and 25 ppm). The percentage of dye removal was assessed in response to sunlight at an average sunlight irradiation of 30 ± 2 °C and under dark conditions. A constant sample weight (2.5 mg) and dye volume (10 mL) were used for this investigation. The removal of dye was measured in the dark to estimate the adsorption of dye by the sample, and this value was subtracted from the total dye removal. The decantation process was employed to separate the membrane from the solution. The remaining dye concentration was determined using a UV–visible spectrophotometer at a wavelength of 668 nm. The results are reported as the mean of triplicate experiments.

The photodegradation efficiency and the adsorption of dye were calculated by the following equation [20–22]:

$$R = \frac{C_0 - C_t}{C_0} \times 100 \quad (1)$$

where C_0 and C_t denote the initial and final dye concentrations at reaction time t.

3. Results and Discussion

In this study, we tried to further expand our previous knowledge in the use of pure formic acid solutions of biodegradable PHB, and explore both their chemical reactivity and the increased polarity compatibilization property of the FA solvent shown during the electrospinning process of pure PHB and PHB/in situ polyvinylformate or PHB/polyamide-6 mats containing dispersed layered silicate protonated montmorillonite nanosheets, demonstrating their potential use in wastewater purification [15,16]. The photocatalytic degradation of polluting textile dyes in industrial wastewater using biodegradable polyesters, such as polyhydroxybutyrate incorporating photocatalyst nanoparticles, is an emerging area of research. This approach utilizes reusable, self-supporting electrospun membranes with a high surface area and well-structured photocatalyst nanoparticles [23]. The inexpensive and easy-to-prepare zinc oxide and titanium oxide nanoparticles (NPs) have a wide direct energy band gap ranging from 3 to 3.5 eV, making them photoactive under UV illumination. This property allows them to generate reactive oxygen species (ROS), which are effective for the chemical decontamination of organic dyes. These nanoparticles are widely studied and explored, both in their bare form and more extensively when embedded and immobilized within polymer or ceramic substrates [24–28]. In this regard, our material properties prescreening rejected the experimental use of zinc oxide NPs, as their amphoteric property and reactivity towards formic acid— forming soluble zinc formate salt—revealed this approach to be fully inappropriate. The preliminary experiments with fully acid-stable commercial TiO_2 anatase nanoparticles (avr. diameter of 10–20 nm) and their compatibilization with formic acid solutions of PHB were unsatisfactory. Both pure FA and PHB/FA solution dispersions showed colloidal instability, with the occurrence of relatively quick particle agglomeration and partial solution sedimentation before and during electrospinning experiments. The only UV-region photoactivation was another known intrinsic disadvantage of the use of anatase TiO_2 NPs; therefore, another idea arose for the use of pure formic acid. Referring to the pioneering study by Campostrini et al., the reactive solvent used in the sol–gel polycondensation reaction of a common titanium (IV) butoxide precursor creates a mixed amorphous titanium alkoxide phase. This phase is effectively compatibilized with both the FA solvent and the PHB macromolecule constituents during the electrospinning

process. In their pyrolysis study protocol of sol–gel-derived TiO_2 powders, Campostrini et al. use a high concentration of titanium (IV) isopropoxide precursor preliminarily dissolved in a 2-propanol solvent and performed a sol–gel reaction by adding a minor amount of formic acid, with the subsequent addition of 1M hydrochloric acid solution, in order to obtain a precursor amorphous titania gel network. The combined MS/GS analysis determined the phase composition corresponding to the mixed titania alkoxide-formate ester phase with the nominal formula $TiO_{1.30}(OH)_{0.64}(OCH(CH_3)_2)_{0.61}(OCOH)_{0.14}$ [8].

In our experimental approach, in order to prepare a discrete nanoparticle phase instead of a bulk 3D network gel, a minor Ti (IV) butoxide precursor fraction was reacted with a highly diluted precursor-to-solvent weight ratio of 1:50 without low-alcohol and hydrochloric acid addition. The intent was to obtain a mixed titania-alkoxyde-formate ester nanoparticle phase, $TiO_x(OH)_y(OC_4H_9)_z(OCOH)_z$, shortly denoted as TiFA. Indeed, the very first experiments of reacting Ti (IV) butoxide with FA under short ultrasound treatment successfully led to the formation of white, colloidally stable dispersions of TiFA NPs. The hypothesis is that the TiFA phase, with a possibly linear oligomeric structure, will exhibit high colloidal dispersion stability and structural coordination with the PHB polyester macromolecules and facilitate composite solution electrospinning, as illustrated in the general material preparation Scheme 1:

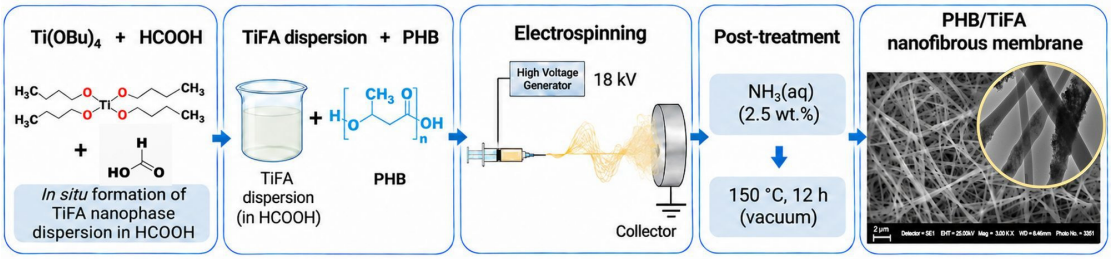

Scheme 1. Preparation of composite electrospun PHB/TiFA mats.

As the embedment of the structurally complex and not unambiguously determined TiFA nanophase composition in the electrospun composite PHB fibrous mats could raise some concerns in strict composition-ratio pre-determination, we chose to designate the obtained PHB/TiFA composite mats with the theoretical 5 and 10 wt.% pure TiO_2 content on the basis of the amount of initial Ti (IV) butoxide precursor loading. In order to study the possible physico-chemical and structural changes in both the isolated TiFA NPs and the electrospun composite PHB/TiFA fibers, they were also subjected to room-temperature 2.5 wt. % ammonia solution treatment (PHB/Ti NH_3 samples) and to heat treatment at 150 °C (PHB/Ti NH_3 sample), which is below the melt diapason of neat PHB. The ammonia treatment was intended to partially hydrolyze the organo-titanium nanophase and remove part of the butoxide and formate ester groups for an exchange of surface Ti-OH group enrichment. The presumption of relatively low-temperature heat treatment of the obtained PHB/TiFA composites was mostly to induce physical and, to a lesser extent, chemical dehydration processes, as well as structural reinforcement. Another crucial parameter of the newly prepared polytitanate NPs and the electrospun nanocomposites was the investigation of the atomic Ti^{3+}/Ti^{4+} ratios in the different obtained samples.

3.1. Characterization of Polyhydroxybutyrate Electrospun Fibrous Membranes Loaded with Amorphous Titania Nanophase

3.1.1. Surface Composition and Valence State Analysis

X-ray photoelectron spectroscopy (XPS) was used to determine the composition and chemical state of the elements on the surface of electrospun composite membranes. The

analysis of membranes with the polymer shows that C1s, O1s, Ti2p, and N1s peaks were registered on the surface (Figure 1). The amounts of these chemical elements in atomic concentrations are shown in Table 1. The shape and width of the carbon spectra show several peaks that are attributed to the bonds C-C, C-O/C-N, and C=O. The carbon–oxygen bonds are also confirmed by the deconvoluted spectra of O1s. The spectrum of oxygen (Figure 1) is broad and decomposes into multiple components: oxygen bound to titanium (530.0 eV), a carbonyl group (531.3 eV), hydroxyl groups adsorbed on the surface (532.2 eV)—OH groups related to the PHB polymer matrix and a small number of hydroxyl groups bound to the titanium phase [29]—the ester functional group C-O (533.3 eV), and oxygen in the chemisorbed water molecules (534.2 eV). The binding energies of the decomposed peaks of the C and O spectra, as well as their concentrations up to 100%, are presented in Table 2. The surface concentration of titanium was relatively low across all samples, remaining at or below approximately 0.9 at.%. Despite this low overall content, the high-resolution Ti2p spectra clearly exhibited two distinct oxidation states [30] after deconvolution with Gaussian–Lorentzian curve fitting: Ti^{3+} (binding energies at 457.5 eV for Ti $2p_{3/2}$ and 463.2 eV for Ti $2p_{1/2}$ with spin-orbit splitting of $\Delta = 5.7$) and Ti^{4+} (binding energies at 458.7 eV for Ti $2p_{3/2}$ and 464.4 eV for Ti$2p_{1/2}$, $\Delta = 5.7$). The FWHM values were fixed at 1.6 eV for Ti $2p_{3/2}$ and 1.8 eV for Ti$2p_{1/2}$, and the ratio of their areas is 2 to 1. The percentage distribution of these two oxidation states is detailed in Table S1. The Ti^{4+} oxidation state primarily corresponds to TiO_2, but it is likely also correlated with the formation of $Ti(OH)_4$ species, which is strongly supported by the prominent hydroxyl contribution identified in the deconvoluted O1s spectra. For the ammonia-treated samples (PHB/TiFA 5 NH_3-RT and PHB/TiFA 5 NH_3-150 °C), a minor amount of nitrogen (below 1 at.%) was successfully registered on the surface, confirming the effective surface interaction and chemical activation induced by the basic treatment.

Table 1. XPS results on the surface of the prepared PHB/TiFA composite fibers.

Samples	C, at. %	O, at. %	Ti, at. %	N, at. %
PHB/TiFA 5 NH_3-150 °C	67.1	31.4	0.9	0.6
PHB/TiFA 10	71.3	28.5	0.2	-
PHB/TiFA 5 NH_3-RT	68.7	30.2	0.4	0.7
TiFA 5 NH3-150 °C	17.1	59.8	23.1	-
TiFA	18.9	55.9	21.7	3.4
TiFA 5 NH3-RT	19.3	54.3	22.8	3.6

Table 2. EDS results of polyhydroxybutyrate electrospun fibrous membranes loaded with TiFA nanophase.

Atomic %	**C**	**O**	**Ti**	**Total**
PHB-0	89.98	10.02	-	100.00
PHB/TiFA 5 NH_3	67.06	32.04	0.91	100.00
PHB/TiFA 10 NH_3	86.34	13.47	0.19	100.00
Wt %	**C**	**O**	**Ti**	**Total**
PHB-0	87.09	12.91	-	100
PHB/TiFA 5 NH_3	59.16	37.65	3.19	100
PHB/TiFA 10 NH_3	82.19	17.08	0.73	100

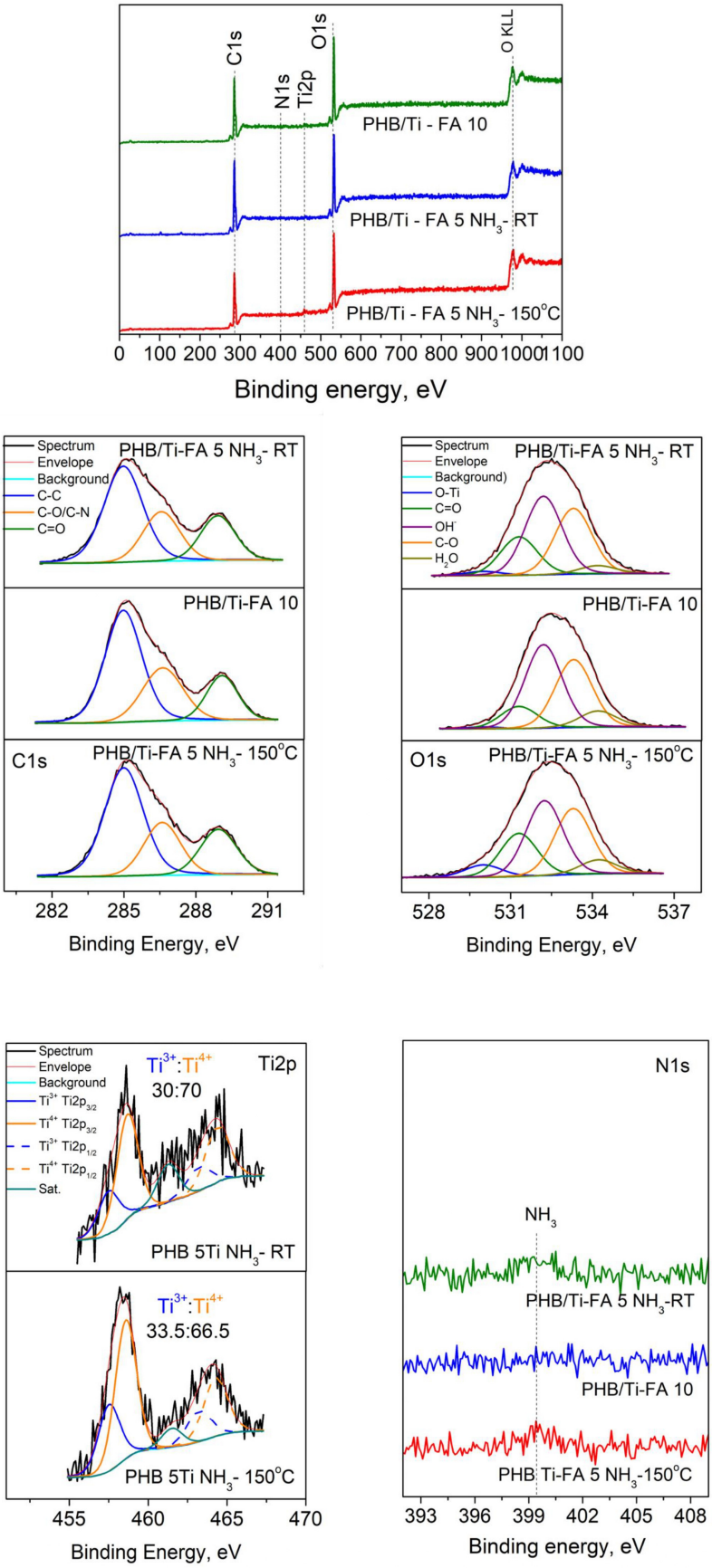

Figure 1. Survey spectra and deconvolution of C1s, O1s, Ti2p, and N1s core-level spectra of the electrospun PHB/TiFA mats.

XPS analysis was also performed on membranes without the polymers TiFA, TiFA 5 NH_3-RT, and TiFA 5 NH_3-150 °C. The wide-scan spectra confirmed the presence of C1s, O1s, Ti2p, and N1s photoelectron peaks on the analyzed surfaces (Figure 2). The quantitative atomic concentrations of these elements are summarized in Table 1.

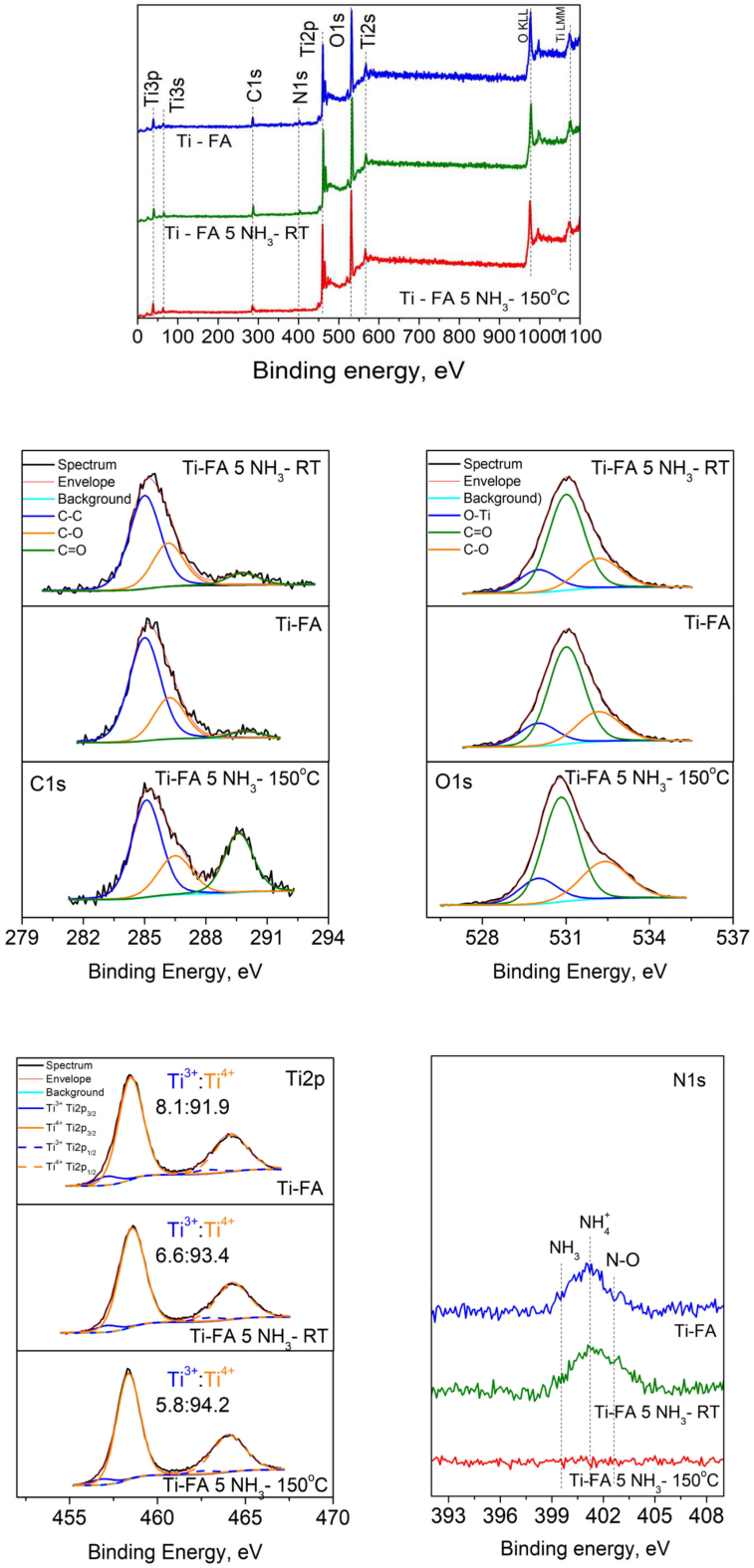

Figure 2. Survey spectra and deconvolution of Ti2p core-level spectra of different treated TiFA samples.

The deconvolution of the high-resolution C1s core-level spectra revealed distinct peaks corresponding to C–C (285.0 eV), C–O/C–N (~286.2 eV), and C=O (~289.8 eV) chemical bonds (Table S2). These carbon–oxygen configurations were further corroborated by the high-resolution O1s spectra. The broad O1s profile was successfully deconvoluted into multiple components: oxygen bound to titanium (O–Ti at 530.0 eV), carbonyl groups (C=O at 531.0 eV), and ester functional groups (C–O at ~532.4 eV). Nitrogen at about 3.5 at. % was also registered on the surface. The N1s spectrum reveals contributions attributed to neutral ammonia (NH_3–399.6 eV), ammonium species (NH_4^+–401.3 eV), and an N-O bond (402.6 eV). Following decomposition, the titanium spectra reveal two oxidation states: Ti^{3+} and Ti^{4+}, with spin-orbit splitting of $\Delta = 5.7$ and binding energies at 457.1 eV ($Ti2p_{3/2}$) and 462.8 eV ($Ti2p_{1/2}$), and 458.5 eV ($Ti2p_{3/2}$) and 464.2 eV ($Ti2p_{1/2}$), respectively (Figure 2). Interestingly, after the deconvolution of the control titania samples synthesized without the polymer matrix (the TiFA series), it was found that the concentration of Ti^{3+} decreases approximately 5-fold with a simultaneous increase in the Ti^{4+} fraction. This indicates that the PHB polymer matrix plays a crucial role in stabilizing the reduced Ti^{3+} species within the electrospun fibrous network during the in situ generation process.

3.1.2. Morphological Characteristics

The morphology of the obtained electrospun composite mats was studied by SEM analysis (Figure 3). The determined average fiber diameters are 89 nm ±29 (PHB), 112 nm ± 32 (PHB/TiFA 5 NH_3), and 95 nm ± 31 (PHB/TiFA 10 NH_3), respectively. While the loading of TiFA nanoparticles slightly affects the average diameter of the electrospun mats, the morphology of the obtained composite fibers is positively affected in terms of their deposition density, and a partial decrease in interconnection defects is caused by the slow solvent evaporation rate.

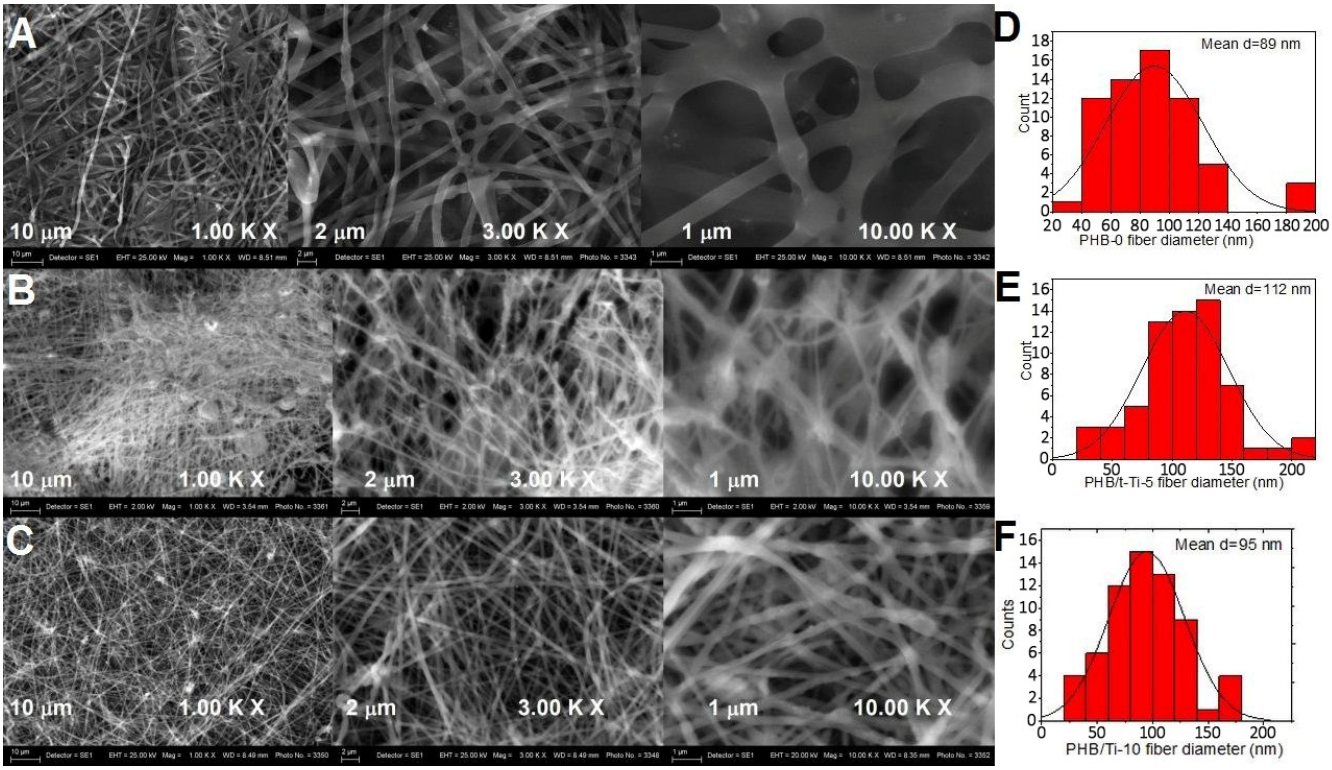

Figure 3. SEM images of (**A**) pure PHB, (**B**) PHB/TiFA 5 NH_3, and (**C**) PHB/TiFA 10 NH_3, and histograms of (**D**) pure PHB, (**E**) PHB/TiFA 5 NH_3, and (**F**) PHB/TiFA 10 NH_3 polyhydroxybutyrate electrospun fibrous membranes loaded with TiFA nanoparticles.

The EDS spectra of pure polyhydroxybutyrate and polyhydroxybutyrate electrospun fibrous membranes loaded with titania (Figure S1) and Table 2 show the presence of C and O for pure PHB and C, O, and Ti peaks for PHB/TiFA, without other elemental impurities. The incorporation of nanoparticles into the nanofibers is shown in Figure 4. TEM images demonstrate the inclusion of titania nanoparticles both within and on the surface of the nanofibers.

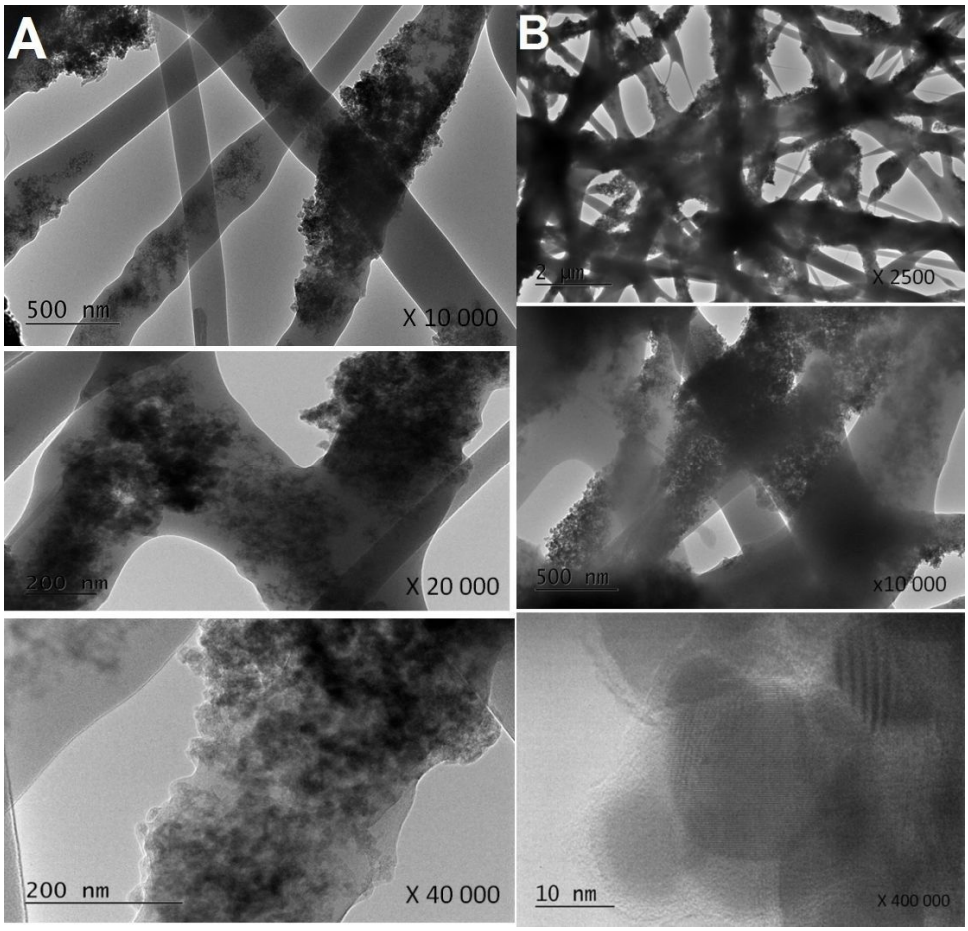

Figure 4. TEM images of (**A**) PHB/TiFA 5 and (**B**) PHB/TiFA 5NH_3 electrospun fibrous membranes loaded with TiFA NPs.

The incorporation of a TiFA nanophase into the PHB fibrous matrix was studied by TEM analysis, as shown in Figure 4.

From the TEM observation, the successful incorporation of discrete TiFA clustered nanoparticles distributed both on the surface and inside the PHB fibers is visible. The high-magnification TEM scans provide direct evidence of our successful processing strategy. Instead of forming large macro-scale agglomerates that typically settle out of solution, the in situ-reacted TiFA intermediate phase organizes into discrete clusters of sub-nanometer particles. These clusters are uniformly distributed both along the thin surface edge boundaries and safely embedded inside the core structural volume of the individual electrospun PHB fibers. TEM and HR-TEM observations (Figure 4) provide definitive evidence of the dispersion state and nanoscale architecture of the incorporated titania nanophase. Low- and medium-magnification images (Figure 4A,B) confirm that the TiFA phase is successfully integrated as discrete, clustered nanoparticles and dense nanocoatings distributed both throughout the interior matrix and along the outer perimeter of the PHB fibers. Crucially, the high-resolution TEM micrograph taken at 400,000× magnification (Figure 4B, bottom) reveals well-defined lattice fringes within localized nanoclusters (5–10 nm). The measured

interplanar fringe spacing is approximately d ≈ 0.35 nm, corresponding closely to the (101) crystallographic plane of the anatase TiO_2 lattice. Bulk WAXD scans detect no macroscopic diffraction peaks, indicating an overwhelmingly X-ray-amorphous organo-titanate network. HR-TEM clearly demonstrates the presence of sub-5 nm crystalline nuclei. The formation of these ordered nanodomains is facilitated by the mild thermal treatment at 150 °C and the preceding basic ammonia-assisted condensation, which promotes localized densification into photoactive anatase seeds without inducing bulk crystallization of the hybrid network.

3.1.3. Thermal Profile and Structural Characteristics

The thermal stability and degradation behavior of the synthesized in situ titania precursors and the electrospun composite membranes were evaluated by thermogravimetric analysis (TGA). Figure 5 illustrates the TG curves of the neat precursors (TiFA and TiFA NH_3) alongside the composite fibrous mats (PHB/TiFA 5 and PHB/TiFA 10) heated up to 800 °C in an argon atmosphere. The pure organo-titanium precursors demonstrate a progressive, multi-step weight loss extending up to approximately 350 °C. This mass reduction is primarily attributed to the evaporation of residual formic acid and unreacted species, followed by the thermal decomposition of the coordinated formate/alkoxy organic groups and the concomitant condensation of the network into a solid inorganic phase. Notably, the ammonia-treated precursor (TiFA NH_3) exhibits a slightly higher residual mass compared to the untreated Ti, suggesting that the basic environment promotes a higher degree of pre-condensation and cross-linking of the titanate network prior to the thermal treatment. Regarding the electrospun composites, pure PHB is known to degrade almost completely in a single narrow temperature step, typically between 250 °C and 300 °C, due to rapid, random chain scission via a *cis*-elimination mechanism. The composite mats (PHB/TiFA 5 NH_3 and PHB/TiFA 10 NH_3) exhibit a nearly identical sharp degradation profile in this exact temperature range. This indicates that the incorporation of the in situ-generated amorphous titania nanophase does not significantly accelerate the thermal degradation or compromise the inherent thermal stability of the PHB polymer matrix. Crucially, the residual mass recorded at 800 °C provides direct confirmation of the successful embedding of the inorganic phase. The PHB/TiFA 10 NH_3 composite exhibits a distinctly higher final inorganic residue compared to the PHB/TiFA 5 NH_3 sample. This proportional increase in the residual mass perfectly aligns with the higher initial loading of the titanium precursor (10 wt.% vs. 5 wt.%), confirming the effective and concentration-dependent in situ generation of the titania nanophase within the electrospun fibers [31,32]. The TGA thermogram of the pure TiFA precursor (added as Supplementary Information Figure S2) shows that the thermal decomposition of the precursor up to 800 °C exhibits a total mass loss consisting of three main steps (16.6%, 26.7%, and 3.3%), leaving a final residual mass of approximately 53.4% (which corresponds to the fully condensed, pure TiO_2 phase). This experimentally determined yield factor (0.534) was the exact mathematical basis used to calculate the required mass of the initial precursor added to the PHB dopes to achieve the theoretical 5 wt.% and 10 wt.% pure TiO_2 loadings in the final composite. The actual bulk incorporation of the inorganic phase is independently confirmed by the TGA of the composites. The residual mass at 800 °C clearly shows that the PHB/TiFA 10 NH_3 composite yields a distinctly higher final inorganic residue compared to the PHB/TiFA 5 NH_3 sample. This proportional increase directly correlates with the higher initial precursor loading and confirms that the bulk material contains the expected higher amount of the organo-titanium phase.

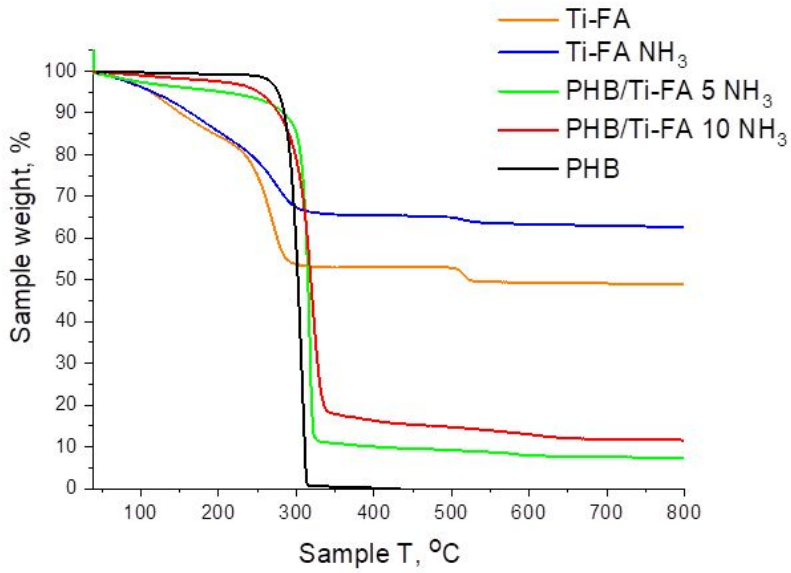

Figure 5. TG curves of PHB, TiFA, TiFA NH_3, PHB/TiFA 5 NH_3, and PHB/TiFA 10 NH_3 polyhydroxybutyrate electrospun fibrous membranes loaded with organo-titanium nanophase.

The onset of the main degradation step above 200 °C validates our choice of a 150 °C thermal treatment for the electrospun mats. This specific temperature is sufficient to remove unbound moisture while preserving the strongly coordinated organo-titanium framework, perfectly aligning with the FT-IR and WAXD observations of the stabilized amorphous phase.

In addition, the TGA-MS analysis of the isolated amorphous TiFA nanofiller (see the SI) that was performed gives us further insights into the phase composition and the chemical nature of the isolated organo-titanate nanopowder. The TiFA thermogravimetric curve showed multi-step mass loss during continuous heating in an argon atmosphere up to 800 °C at a rate of 15 °C/min (Figure S2). The extracted ion chromatograms (Figure S3) of the evolved gases during the thermal degradation confirm the release of water (H_2O), carbon monoxide (CO), and formic acid (HCOOH, m/z 45 and 46) at ~17.1 min (corresponding to ~296 °C), followed by the release of butanol (ButOH) at ~34.0 min (corresponding to ~550 °C). The mass spectrum matched against the NIST library identifies formic acid as a primary degradation product, confirming the presence of coordinated formate and residual butoxide ligands within the hybrid organo-titanium network. Furthermore, the TGA-MS results provide profound insight into the coordination strength of the network. While free formic acid and butanol boil at ~101 °C and ~117 °C, respectively, their delayed release at extremely high temperatures (~296 °C for formate and ~550 °C for butoxide derivatives) conclusively proves that these species are not merely physically trapped solvents, but strongly coordinated chemical ligands.

The crystal structure and phase composition of the pristine PHB and the electrospun composite mats were investigated using wide-angle X-ray diffraction (WAXD), as shown in Figure 6. The diffractogram of the neat PHB displays distinct diffraction peaks at 2θ values of approximately 13.5° and 17.0°, corresponding to the (020) and (110) crystallographic planes of the highly crystalline orthorhombic PHB lattice. Smaller reflections observed between 20° and 30° are also characteristic of the polymer's crystalline domains. For the composite sample prepared at room temperature (PHB/TiFA RT), these characteristic PHB peaks are preserved, indicating that the initial incorporation of the titanium precursor does not drastically alter the polymer's crystal structure. However, upon thermal treatment at 150 °C (PHB/TiFA 150 °C), the intensity of the main crystalline peaks significantly decreases, and the peaks become noticeably broader. This behavior suggests that the applied high-

temperature treatment, combined with the in situ formation of the cross-linked titania network, partially disrupts the crystallization of PHB, leading to a decrease in the overall crystallinity of the polymer matrix. Furthermore, the diffractograms of the composite membranes do not reveal any sharp diffraction peaks corresponding to a highly crystalline TiO_2 phase (such as the intense anatase reflection typically expected around $2\theta \approx 25.3°$). The absence of such reflections confirms that the low-temperature in situ generation and subsequent treatments predominantly yield an amorphous organo-titanium nanophase.

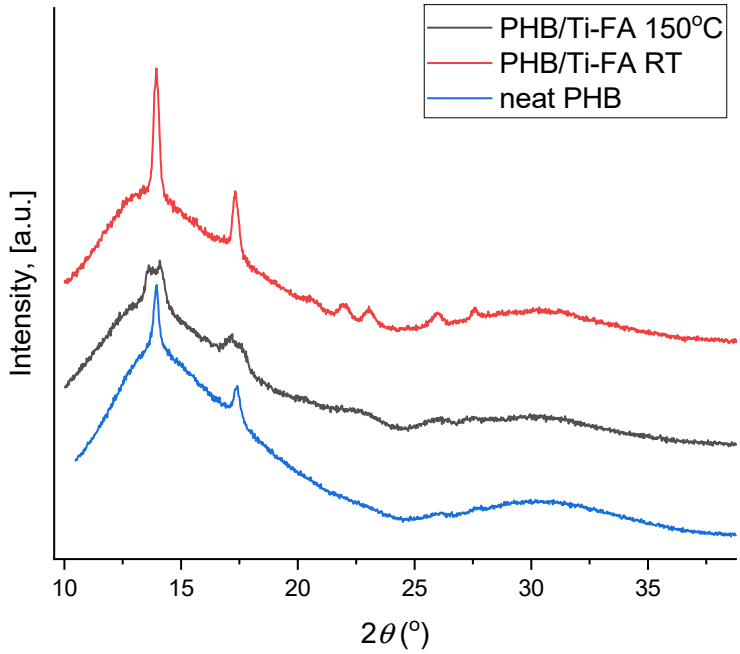

Figure 6. Wide-angle X-ray diffraction patterns of the electrospun PHB/TiFA mats.

Thermal treatment at 150 °C may induce changes in the crystalline organization of PHB through partial melting, crystal reorganization, or recrystallization, depending on the treatment duration and thermal history. These changes may be reflected in the WAXD patterns through variations in diffraction peak intensity and the relative degree of crystallinity. Meanwhile, the TGA results can provide complementary information about the thermal stability of PHB, helping to determine whether the treatment caused any detectable changes in its thermal degradation behavior.

To elucidate the chemical transformation and coordination mechanism of the titanium precursor during the in situ sol–gel process within the formic acid medium, ATR FT-IR spectra of the $Ti(OBu)_4$/FA system were recorded at room temperature, at 150 °C, and at 400 °C (Figure 7). The room-temperature spectrum of the $Ti(OBu)_4$\FA mixture exhibits a characteristic band at 1720 cm^{-1}, corresponding to the C=O stretching vibration of carbonyl groups from the reactive ester or acid species. Crucially, the appearance of two intense bands at 1544 cm^{-1} and 1378 cm^{-1} is assigned to the asymmetric $\nu_{as}(COO^-)$ and symmetric $\nu_a(COO^-)$ stretching vibrations of formate groups coordinated to the titanium center, respectively [33]. The separation between these two frequencies $\Delta\nu = \nu_{as} - \nu_s =$ 166 cm^{-1}, strongly suggests a bridging or bidentate coordination mode of the formate ligands to the titanium atoms (Ti–OOCH). The bands observed in the 1000–1200 cm^{-1} range (e.g., 1129 cm^{-1} and 1052 cm^{-1}) are attributed to the C–O stretching of the alkoxy (butoxy) and formyl groups, while the broad band around 513 cm^{-1} represents the initial formation of Ti–O–Ti oxo-bridges via condensation. Upon thermal treatment at 150 °C, $Ti(OBu)_4$_FA_150 C, which mirrors the conditioning temperature of the composite mats, significant structural alterations occur. The sharp ester/carbonyl band at 1720 cm^{-1} and the

distinct alkoxy bands between 1000 and 1200 cm^{-1} practically disappear, indicating extensive volatilization of volatile components and advanced acidolysis/alkalolysis. Concurrently, the coordinated formate bands shift slightly and broaden into prominent bands at 1546 cm^{-1} and 1360 cm^{-1}. This indicates the formation of a stable polyalkyl titanate or organo-titanium oxo-polymer network that retains coordinated organic ligands up to this temperature, supporting the amorphous nature observed in the XRD analysis. Finally, after calcination at 400 °C, $Ti(OBu)_4$_FA_400 C, the organic functional groups are almost completely decomposed and eliminated, as evidenced by the drastic reduction in the formate bands (1558 cm^{-1} and 1366 cm^{-1}). Most prominently, intense and sharp absorption bands emerge in the low-wavenumber region at 446 cm^{-1} and 418 cm^{-1}. These reflections are unambiguously assigned to the Ti–O–Ti lattice-stretching vibrations, confirming the ultimate conversion of the organo-titanium network into a well-condensed titanium dioxide framework at elevated temperatures [34,35].

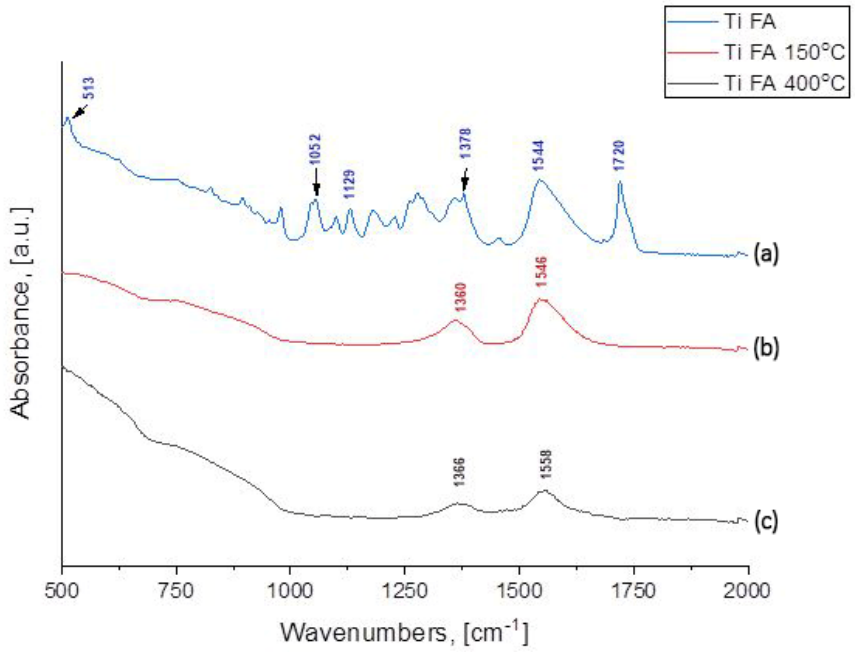

Figure 7. ATR FT-IR analysis of the isolated amorphous (**a**) TiFA powder; (**b**) TiFA powder treated at 150 °C; and (**c**) TiFA powder treated at 400 °C.

To independently validate the FT-IR findings, the TGA-MS analysis of the pure precursor was additionally performed (added as Supplementary Information Figure S3). The mass spectrometry profile of the evolved gases unambiguously detects the release of formic acid (showing a distinct peak at m/z 46, with a 47.7% probability match in the NIST library) during the thermal degradation step.

3.1.4. Surface Wettability

The water contact angles (CA) for the investigated electrospun composite fibrous membranes indicate the extent of wettability, as displayed in Figure 8. The electrospun PHB sample presents a contact angle of 109°, indicating a hydrophobic character for this polymer. Introducing TiO_2 (5 wt. %) to PHB showed a noticeable decrease in the contact angle value to 104°. This behavior points to the hydrophilic nature of TiO_2. It influences the surface of PHB when loaded onto it, with a proportional change in the hydrophobic nature of this composite, leading to slight hydrophilization. As the content of TiO_2 is doubled in PHB, the CA value shows a further decrease to 95°, emphasizing the effect of the hydrophilic tendency of TiO_2. Moreover, the basic treatment of the tested electrospun films

upon being immersed in ammonia showed more hydrophilic behavior than that induced by TiO_2 alone. Ammonia exhibits an intense affinity towards water. Hydrogen bonding takes place between the composite surface and water as a result of activating the polymer surface with NH_3. Hence, the PHB sample loaded with TiO_2 (10 wt. %) and treated with ammonia exhibited the lowest CA value of 86° among the tested films.

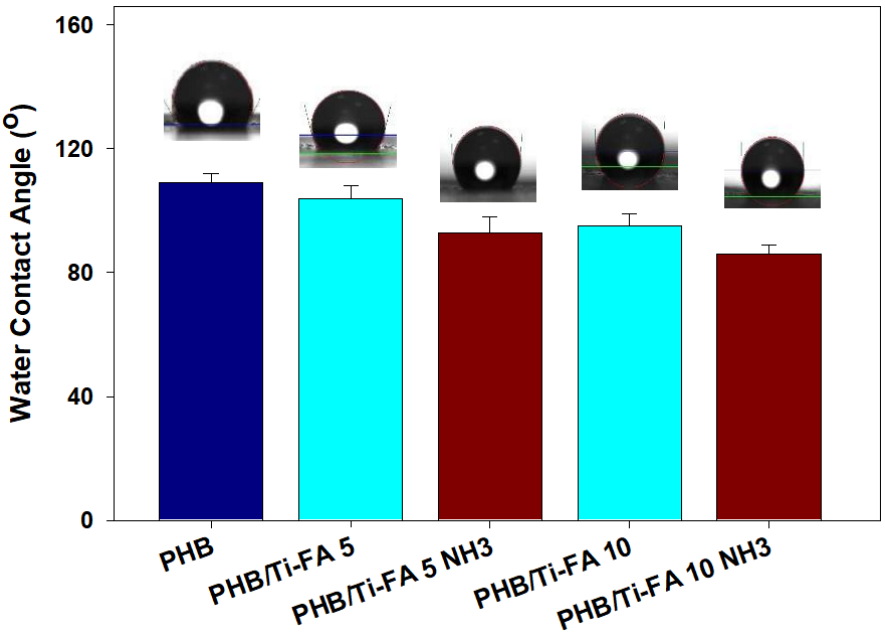

Figure 8. Water contact angles of PHB, PHB/TiFA 5, PHB/TiFA 5 NH_3, PHB/TiFA 10, and PHB/TiFA 10 NH_3 electrospun composite fibrous membranes.

3.1.5. Solar-Driven Photocatalytic Performance and Kinetics

Photocatalytic profiles of the prepared mats are shown in Figure 9. The plots show the effect of TiO_2 concentration on MB degradation. The increase in TiO_2 content from 5% to 10% decreases the photodegradation of MB. This behavior may be attributed to the agglomeration of TiO_2 NPs; they tend to block direct contact with MB molecules. In Figure 9, the effect of basic treatment on mat performance is also shown. The treated mats PHB/TiFA 5 NH_3 and PHB/TiFA 10 NH_3 have higher photocatalytic capacities than the untreated ones. The changes were calculated to be 15% and 16% for PHB/TiFA 10 NH_3 and PHB/TiFA 5 NH_3, respectively. Therefore, PHB/TiFA 5 NH_3 was employed for the following investigations. The alkaline treatment increased the catalysts' porosity and surface area, contributing to a higher density of surface hydroxyl groups [36]. It enhanced the surface area available for reactions as well.

The degradation time is one of the most important factors to evaluate the photocatalytic degradation performance of PHB/TiFA 5 NH_3. As shown in Figure 10, the concentration of the MB solution (10 ppm) decreased continuously upon increasing the time of each experiment (1, 2, 3, 4, and 5 h) in sunlight. After 60 min, almost 60% of the MB concentration substantially declined (Figure 11). After that, the degradation process proceeded, and the photodegradation process reached about 98.4% after 5 h of exposure to sunlight in the presence of PHB/TiFA 5 NH_3 nanofibers.

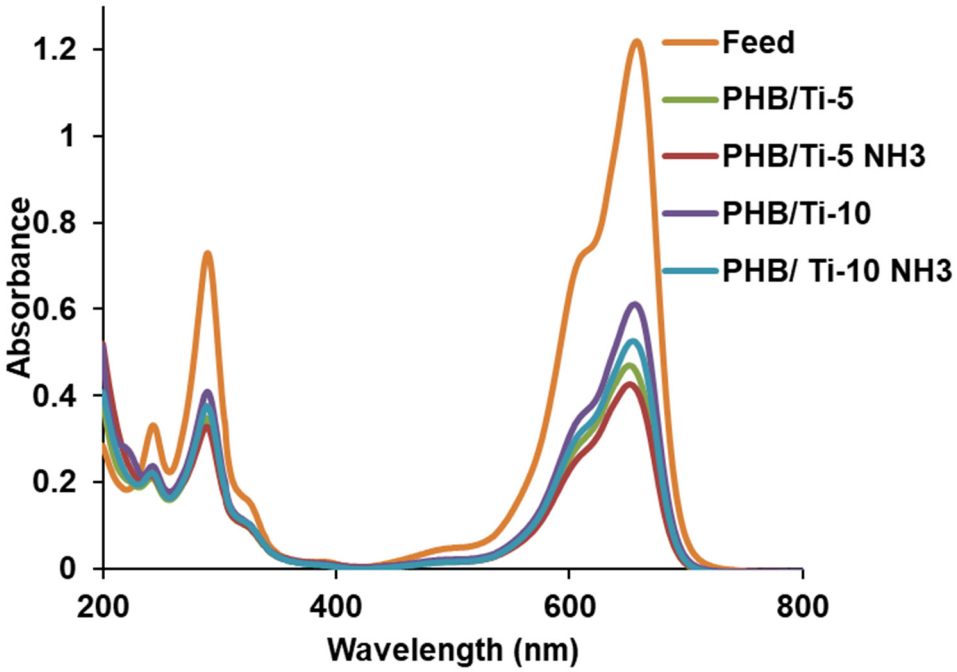

Figure 9. UV–vis spectra of MB solution after treatment by the prepared nanofiber mats in the presence of sunlight for 60 min, where MB feed concentration was 10 ppm.

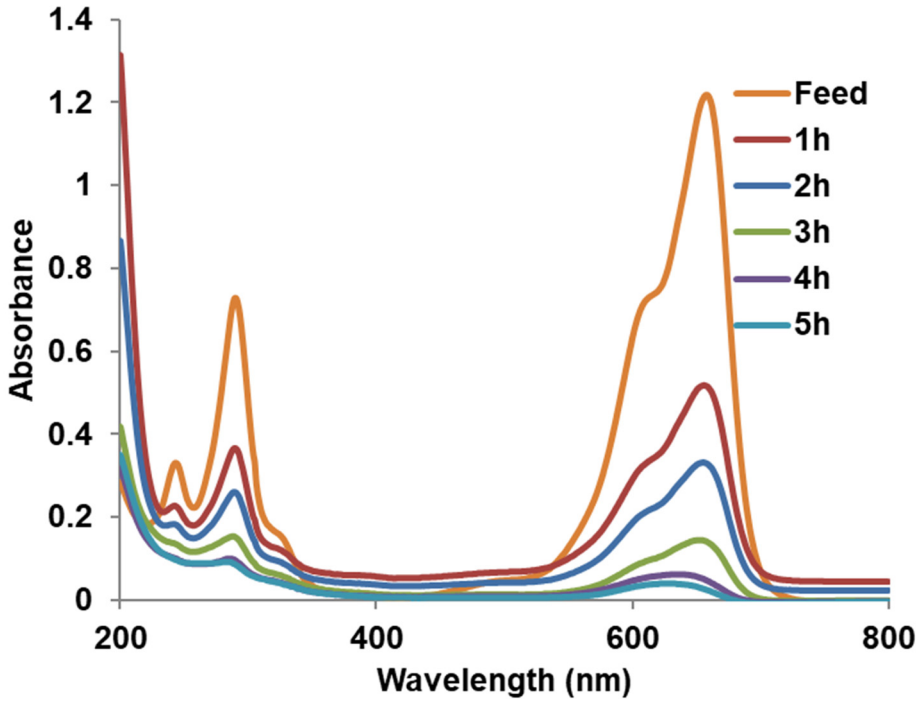

Figure 10. UV–vis scanning spectra of the degradation of MB by PHB/TiFA 5 NH_3 at different time intervals (MB feed concentration: 10 ppm).

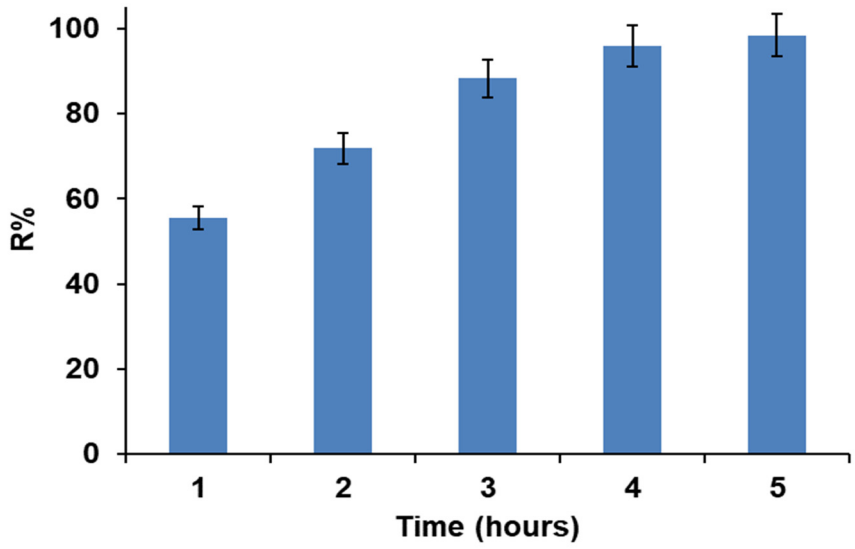

Figure 11. Degradation of MB by PHB/TiFA 5 NH_3 at different times (feed concentration: 10 ppm).

The photodegradation efficiency (R) was calculated according to the following Equation (2) [10,37]:

$$R = \frac{C_0 - C_t}{C_0} \times 100 \quad (2)$$

where C_0 and C_t denote the initial and final dye concentrations for reaction time t.

The effect of initial dye concentration on the photocatalytic performance of PHB/TiFA 5 NH_3 nanofiber mat is shown in Figures 12 and 13. In Figure 12, the UV–vis scanning spectra of different dye concentrations after photodegradation were monitored and displayed a large decline in the dye concentration, even at high concentration (25 ppm). The scanning spectrum decreased considerably compared to the feed solution of 10 ppm (Figure 9). The concentration of the remaining MB dye after the photodegradation process using PHB/TiFA 5 NH_3 under exposure to sunlight was measured and displayed in Figure 13. The degradation effect of nanofiber mats progressed first in the dark to exclude the adsorption properties of PHB/TiFA 5 NH_3. Moreover, it showed low performance, as the removal efficiency of MB decreased from about 40 to 7.2% when increasing the dye concentration from 5 to 25 ppm. In contrast, the photodegradation efficiency of the nanofiber mats under sunlight decreased from 98.4 to 78% for the MB dye as the concentration increased from 5 to 25 ppm, respectively, after 3 h. These results indicate the high-performance properties of the prepared PHB nanofiber incorporating TiO_2 nanoparticles as a photocatalytic candidate for the degradation of MB dye under daylight irradiation [38].

Figure 14 displays a digital photo of the different dye concentrations before and after the photodegradation process. As shown in the image, the color of the dye significantly decreased after being exposed to visible sunlight in the presence of PHB/TiFA 5 NH_3, which resulted in the photodegradation of MB dye molecules.

The Langmuir–Hinshelwood (LH) kinetic model serves to explain heterogeneous catalysis. The reaction rate depends on the concentration of the pollutant, as expressed in the following equation [39]:

$$r = \frac{dC}{dt} = \frac{-kKC}{1 + KC} \quad (3)$$

where r denotes the reaction rate; C is the concentration of dye in the solution; t stands for time; k is the reaction constant; and K is the adsorption equilibrium factor for the pollutant on the photocatalyst's surface. The equation can be simplified by neglecting KC to be

$$ln\left(\frac{C_0}{C}\right) = K_a \cdot t \quad (4)$$

where C_0 and C are the initial concentration of MB and at a specific time t; and $Ka = -kK$ (h^{-1}) is the rate constant of the pseudo-first-order model [40].

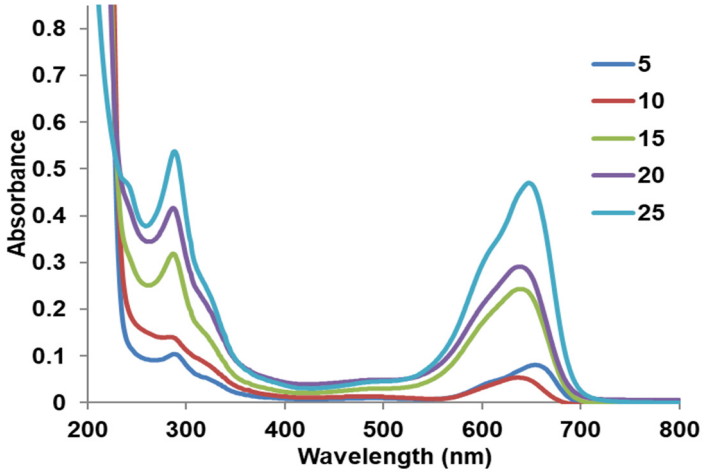

Figure 12. Effect of initial dye concentration on the photocatalytic degradation effect of PHB/TiFA 5 NH_3 on MB after 5 h.

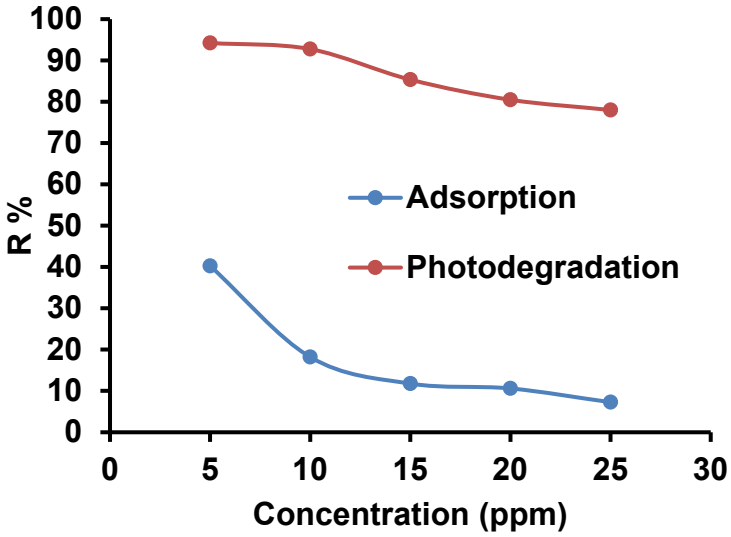

Figure 13. Effect of initial dye concentration on the removal and photodegradation efficiency of PHB/TiFA 5 NH_3 for MB after 3 h.

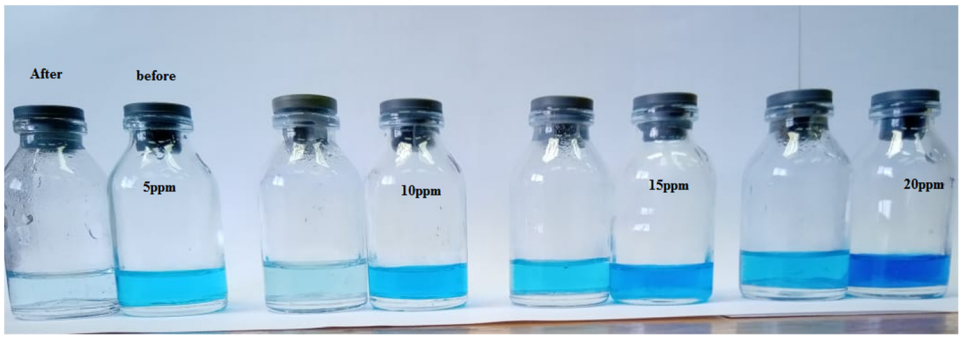

Figure 14. A digital photo of different dye concentrations before and after degradation in sunlight for about 5 h.

The kinetic study of MB photodegradation in an aqueous solution using nanofiber mats of PHB/TiFA 5 NH_3 was assessed using the commonly applied pseudo first-order Equation (4).

The graphs of $\ln(C_0/C)$ were plotted as a function of the reaction time, as shown in Figure 15. The linearization of the results confirms the well-fitted pseudo-first-order kinetics of the photodegradation of MB dye using PHB/TiFA 5 NH_3, with $R^2 = 0.9842$ and the rate constant Ka: 0.8556 h^{-1}. These findings indicate the relative speed of the photodegradation process. The photodegradation of the MB dye in the solution is initiated by the photoexcitation of the treated TiO_2 nanoparticles embedded in PHB nanofibers, followed by the production of an electron–hole pair on the surface of the TiO_2 catalyst. The high oxidative potential of the valence-band holes (h + VB) in the TiO_2 and hydroxyl radicals allows the instantaneous oxidation of the organic dye (MB), forming reactive intermediates followed by complete degradation [41].

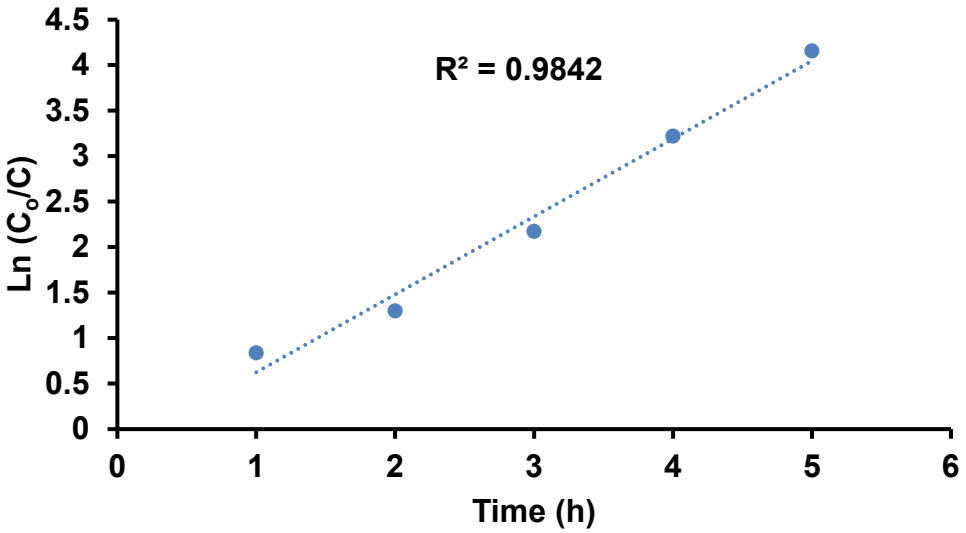

Figure 15. Fitting of pseudo-first-order kinetics of PHB/TiFA 5 NH_3 towards MB degradation (MB feed concentration is 10 ppm and time duration is 5 h under sunlight).

The apparent pseudo-first-order rate constant for MB degradation was $k = 0.856$ h^{-1}, $R^2 = 0.9842$, $n = 3$. Based on the fitted data, the estimated uncertainty was approximately 0.108 h^{-1}. To explore whether experimental degradation data follow second-order kinetics, the Integrated Rate Law was applied:

$$\frac{1}{C_t} = \frac{1}{C_0} + k_2\, t$$

which can be represented in a linearized form as follows:

$$\frac{t}{C_t} = \frac{t}{C_0} + \frac{1}{C_0 k_2}$$

where C_0 is the initial concentration of the pollutant at t = 0; C_t is the concentration of the pollutant at time t; k_2 is the pseudo-second-order rate constant; and t is the irradiation time.

The data points are scattered far from the linear regression trendline ($R^2 = 0.7448$), indicating that second-order kinetics is not suitable to describe this photocatalytic degradation reaction. Figure 16 shows that after 4 and 5 h of degradation, the concentration of methylene blue (MB) decreased. Its absorbance was measured in the Beer's law region, where it is less than 0.2.

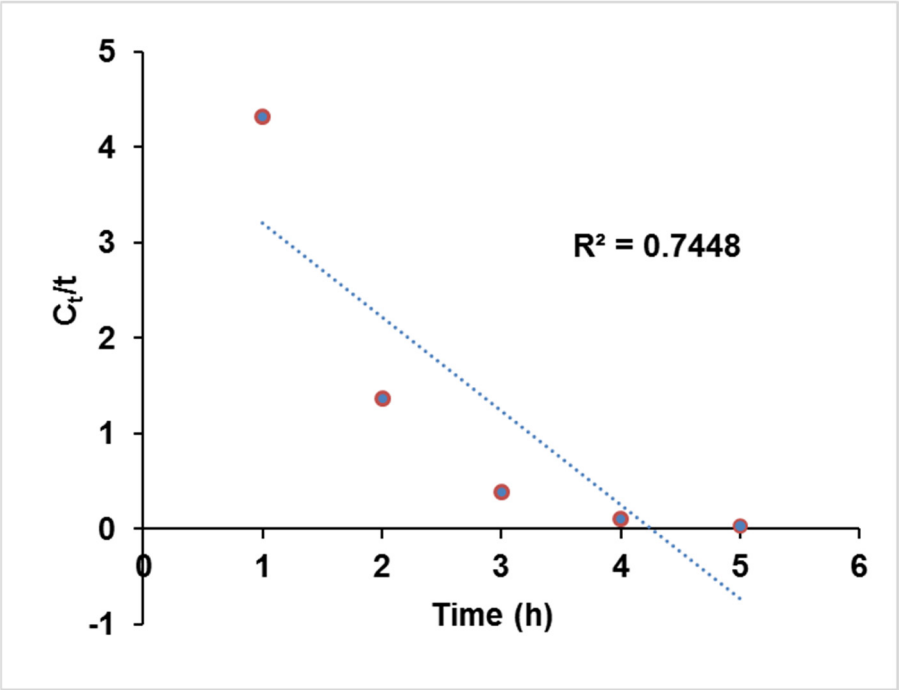

Figure 16. Fitting of pseudo-second-order kinetics of PHB/TiFA 5 NH_3 towards MB degradation with feed concentration of 10 ppm after 5 h.

Table 3 presents the results on the removal of MB dye in order to compare the performance of the developed material in the present study with that of previously reported materials in the literature.

Table 3. The removal of MB dye using the developed material in this work compared with that of reported materials in the literature.

Photocatalyst/System	Light Source	MB Concentration	Catalyst Dosage	Irradiation Time	MB Removal%	k (min^{-1})	Ref.
Cellulose acetate impregnated with ZnO nanoparticles	Sunlight	50 ppm	1 g/L	2 h	75%	0.0114	[42]
ZnO/biochar nanocomposite	Sunlight	10 ppm	1 g/L	120 min	92%	0.0233	[43]
Cu-Cu_2O-Cu_3N nanoparticle mixtures	Visible light, sun-driven	5 ppm	0.25 g/L	6 h	92–96%	Not reported	[44]
$C_3N_4/Ca_2Fe_2O_{5)}$	Natural sunlight	3.5 ppm	0.5 g/L	120 min	96%	0.0580	[45]
Exfoliated g-C_3N_4/Fe_3O_4	Visible light + H_2O_2	20 ppm	0.5 g/L	120 min	90%	0.0156	[46]
TiO_2/ZnO	UV light	6000 ppm	NS	240 min 4 h	94%	0.0120	[47]
CrMo6/TiO_2	UV irradiation	10 ppm	NS	5 h	83.7%	0.006	[48]
Ti-ZnO	UV lamp (λ~365 nm, 4.5 W/m^2)	5 ppm	1 g/L	(150 min) 2.5 h	NS	0.00254	[49]
Polyhydroxybutyrate/TiFA nanofibrous membrane	Sunlight	10 ppm	(0.25 g/L)	5 h	94.4%	0.01426	This work

From the comparison of the different photocatalysts investigated, a brief conclusion can be made regarding the kinetic perspective on photocatalytic dye degradation activity of the newly prepared hybrid nanofibrous membranes with incorporated mixed-valence TiFA organo-titanate nanoparticles, and the self-supporting high-aspect-ratio composite mats.

4. Conclusions

In this study, novel biodegradable nanocomposite fibrous membranes based on polyhydroxybutyrate (PHB) loaded with an in situ-generated amorphous titania nanophase were successfully fabricated via green electrospinning from pure formic acid dopes. Formic acid served as both an effective solvent for PHB and an active sol–gel reaction medium for titanium (IV) butoxide polycondensation and the resulting mixed-valence organo-titanate nanoparticles. Post-spinning alkaline treatment with aqueous ammonia and thermal conditioning preserved an amorphous organo-titanate network enriched with surface hydroxyl groups and stabilized mixed Ti^{3+}/Ti^{4+} valence states within the polymer matrix. Incorporation of the TiFA nanophase improved fiber deposition uniformity, enhanced surface hydrophilicity (reducing water contact angle from 109° down to 86°), and maintained the bulk thermal stability of the PHB matrix. The composite membranes exhibited exceptional daylight photocatalytic degradation of MB, reaching up to 98.4% dye elimination after 5 h following pseudo-first-order kinetics (apparent rate constant Ka = 0.8556 h^{-1}). The 5 wt.% TiFA-loaded, ammonia-treated membrane PHB/TiFA 5 NH_3 showed superior performance over higher loadings due to minimal particle agglomeration and optimal active site exposure. These self-supporting, biodegradable hybrid membranes represent a promising and environmentally sound platform for solar-assisted wastewater remediation.

Further studies on the performance of nanofiber membranes in practical wastewater treatment applications and their scalability should be assessed, considering the economic feasibility of large-scale deployment.

Supplementary Materials: The following supporting information can be downloaded at: https://www.mdpi.com/article/10.3390/membranes16120405/s1, Figure S1: EDS spectra of (A) pure PHB and (B) PHB/TiFA 5 NH3; (C) PHB/TiFA 10 NH3 polyhydroxybutyrate electrospun fibrous membranes loaded with TiFA nanophase; Figure S2: TG curve of the isolated TiFA nanopowder exhibiting the multi-step mass loss during continuous heating in an argon atmosphere up to 800 °C at a rate of 15 °C/min; Figure S3: TGA/GC/MSD analysis of isolated TiFA nanopowder showing the identified thermal degradation products in the range 120–550 °C; Table S1: The percentages of C, O and Ti from various species; Table S2: The percentages of Ti from various species.

Author Contributions: Conceptualization, H.P. and A.M.K.; methodology, H.P. and A.M.K.; validation, A.M.K., A.E.A., E.A.A. and H.P.; formal analysis, A.M.K., A.E.A., E.A.A., F.U., D.B., K.Z., M.S. and O.D.; investigation, A.M.K., A.A.E.-S., A.E.A., E.A.A., H.P., D.B., F.U., K.Z., M.S. and O.D.; resources, A.M.K. and H.P.; data curation, A.M.K., A.E.A., E.A.A. and H.P.; writing—original draft preparation, A.M.K., H.P., K.Z., F.U., S.D., M.S. and D.B.; writing—review and editing, A.M.K., A.A.E.-S., A.E.A., E.A.A., H.P. and K.Z.; visualization, A.M.K., F.U., K.Z. and D.B.; supervision, A.M.K. and H.P.; project administration, A.M.K. and H.P.; funding acquisition, A.M.K. and H.P. All authors have read and agreed to the published version of the manuscript.

Funding: This research was funded by the Bulgarian Ministry of Education and Science under grant agreement N° D01-385/D01-106 18.12.2020; Bulgarian National Science Fund, project KP-06-N69/8 and the Egyptian Academy of Scientific Research & Technology (ASRT), grant number 10115 (Egypt)/IC-EG/05/2022–2024 (Bulgaria).

Institutional Review Board Statement: Not applicable.

Informed Consent Statement: Not applicable.

Data Availability Statement: The original contributions presented in this study are included in the article/Supplementary Material. Further inquiries can be directed to the corresponding authors.

Acknowledgments: The authors (H.P., K.Z., S.D., O.D., and M.S.) express their gratitude to the project with the Bulgarian National Science Fund, KP-06-N69/8 (КП-06-Н69/8), for the financial support. Part of this study was performed in the framework of a joint bilateral project between the Egyptian Academy of Scientific Research & Technology (ASRT) and the Bulgarian Academy of Sciences (BAS)

and with equipment included in the National Infrastructure "ESHER", supported by the Bulgarian Ministry of Education and Science.

Conflicts of Interest: The authors declare no conflicts of interest.

References

1. Yew, S.-P.; Tang, H.-Y.; Sudesh, K. Photocatalytic Activity and Biodegradation of Polyhydroxybutyrate Films Containing Titanium Dioxide. *Polym. Degrad. Stab.* **2006**, *91*, 1800–1807. [CrossRef]
2. Heitmann, A.P.; Rocha, I.C.; Pereira, I.M.; Oliveira, L.C.A.; De Oliveira Patrício, P.S. Nanoparticles of Niobium Oxyhydroxide Incorporated in Different Polymers for Photocatalytic Degradation of Dye. *J. Polym. Res.* **2019**, *26*, 159. [CrossRef]
3. Bhattacharyya, S.; Heran, M.; Chakraborty, S.; Calabro, V.; Algieri, C. Enhancing the Efficiency of Photocatalytic Membrane Reactors for Textile Effluent Remediation. *Sep. Purif. Technol.* **2025**, *375*, 133714. [CrossRef]
4. Heitmann, A.P.; Patrício, P.S.O.; Coura, I.R.; Pedroso, E.F.; Souza, P.P.; Mansur, H.S.; Mansur, A.; Oliveira, L.C.A. Nanostructured Niobium Oxyhydroxide Dispersed Poly (3-Hydroxybutyrate) (PHB) Films: Highly Efficient Photocatalysts for Degradation Methylene Blue Dye. *Appl. Catal. B Environ.* **2016**, *189*, 141–150. [CrossRef]
5. Bhattacharyya, S.; Cozzolino, V.; Dutta, A.; Algieri, C.; Calabrò, V.; Figoli, A.; La Russa, M.F.; de Santo, M.P.; Chakraborty, S. Coupling Photocatalytic Membrane Engineering with Machine Learning for Predictive Fouling Management in Real Pharmaceutical Wastewater. *J. Water Process Eng.* **2026**, *85*, 109800. [CrossRef]
6. Singh, S.; Mahalingam, H.; Singh, P.K. Polymer-Supported Titanium Dioxide Photocatalysts for Environmental Remediation: A Review. *Appl. Catal. A Gen.* **2013**, *462–463*, 178–195. [CrossRef]
7. Hayat, M.; Ahmed, T.; Saleem, A.; Gul, I.; Noor, U.; Bukhari, A.; Yasir, M.; Nasir, A. Black Titania: An Emerging Engineered Material with Advanced Synthesis Strategies and Applications. *Inorg. Chem. Commun.* **2026**, *189*, 116763. [CrossRef]
8. Campostrini, R.; Ischia, M.; Palmisano, L. Pyrolysis Study of Sol-Gel Derived TiO_2powders: Part I. TiO_2-Anatase Prepared by Reacting Titanium (IV) Isopropoxide with Formic Acid. *J. Therm. Anal. Calorim.* **2003**, *71*, 997–1010. [CrossRef]
9. McAdam, B.; Brennan Fournet, M.; McDonald, P.; Mojicevic, M. Production of Polyhydroxybutyrate (PHB) and Factors Impacting Its Chemical and Mechanical Characteristics. *Polymers* **2020**, *12*, 2908. [CrossRef] [PubMed]
10. Kavitha, G.; Rengasamy, R.; Inbakandan, D. Polyhydroxybutyrate Production from Marine Source and Its Application. *Int. J. Biol. Macromol.* **2018**, *111*, 102–108. [CrossRef] [PubMed]
11. Xue, J.; Wu, T.; Dai, Y.; Xia, Y. Electrospinning and Electrospun Nanofibers: Methods, Materials, and Applications. *Chem. Rev.* **2019**, *119*, 5298–5415. [CrossRef] [PubMed]
12. Nagiah, N.; Madhavi, L.; Anitha, R.; Anandan, C.; Srinivasan, N.T.; Sivagnanam, U.T. Development and Characterization of Coaxially Electrospun Gelatin Coated Poly (3-Hydroxybutyric Acid) Thin Films as Potential Scaffolds for Skin Regeneration. *Mater. Sci. Eng. C* **2013**, *33*, 4444–4452. [CrossRef] [PubMed]
13. Ublekov, F.; Budurova, D.; Staneva, M.; Natova, M.; Penchev, H. Self-Supporting Electrospun PHB and PHBV/Organoclay Nanocomposite Fibrous Scaffolds. *Mater. Lett.* **2018**, *218*, 353–356. [CrossRef]
14. Budurova, D.; Ublekov, F.; Penchev, H. The Use of Formic Acid as a Common Solvent for Electrospinning of Hybrid PHB/Soy Protein Fibers. *Mater. Lett.* **2021**, *301*, 130313. [CrossRef]
15. Penchev, H.; Abdelhamid, A.; Ali, E.; Budurova, D.; Grancharov, G.; Ublekov, F.; Koseva, N.; Zaharieva, K.; El-Sayed, A.; Khalil, A. Novel Electrospun Composite Membranes Based on Polyhydroxybutyrate and Poly(Vinyl Formate) Loaded with Protonated Montmorillonite for Organic Dye Removal: Kinetic and Isotherm Studies. *Membranes* **2023**, *13*, 582. [CrossRef] [PubMed]
16. Penchev, H.; Budurova, D.; Ublekov, F.; Zaharieva, K.; Ali, E.A.; Abdelhamid, A.E.; El-Sayed, A.A.; Khalil, A.M. Formic Acid Electrospun Composite Fibers Based on Polyhydroxybutyrate/Polyamide 6 Loaded with Protonated Montmorillonite as Promising Disposable Heavy Metal Removal Sorbent. *Emergent Mater.* **2025**, *8*, 2451–2462. [CrossRef]
17. Khalil, A.M. Recent Advances in Membrane Filtration and Purification Technologies. *Membranes* **2026**, *16*, 78. [CrossRef] [PubMed]
18. Korina, E.; Stoilova, O.; Manolova, N.; Rashkov, I. Polymer Fibers with Magnetic Core Decorated with Titanium Dioxide Prospective for Photocatalytic Water Treatment. *J. Environ. Chem. Eng.* **2018**, *6*, 2075–2084. [CrossRef]
19. Spasova, M.; Stoilova, O.; Manolova, N.; Rashkov, I.; Naydenov, M. Electrospun Eco-Friendly Materials Based on Poly(3-Hydroxybutyrate) (PHB) and TiO_2 with Antifungal Activity Prospective for Esca Treatment. *Polymers* **2020**, *12*, 1384. [CrossRef] [PubMed]
20. Nasr, R.A.; AboBakr, E.; El, G.T.; Mousa, S.M. Harnessing Eco-Friendly Hydroxyapatite/Polyvinyl Alcohol/Whey Protein Bio-Composites for Effective Dye Remediation. *J. Ind. Eng. Chem.* **2026**, *162*, 757–770. [CrossRef]
21. Nasr, R.A.; Ali, E.A.B.; EL-Tawil, R.S. Development of a Natural Mesoporous Feldspar-Polyvinyl Alcohol Composite Film as a Green and Sustainable Adsorbent for Textile Dyes. *J. Taiwan Inst. Chem. Eng.* **2025**, *175*, 106252. [CrossRef]

22. Zhang, S.; Cai, M.; Wu, J.; Wang, Z.; Lu, X.; Li, K.; Lee, J.-M.; Min, Y. Photocatalytic Degradation of TiO_2 via Incorporating Ti_3C_2 MXene for Methylene Blue Removal from Water. *Catal. Commun.* **2023**, *174*, 106594. [CrossRef]
23. Ali, S.; Isha; Aristya, G.R.; Nasir, M.; Zhao, Y.; Areeba; Chang, Y.-C. A Comprehensive Review of Polyhydroxybutyrate (PHB) Composites in Environmental Sustainability: Applications and Future Prospects. *Macromol* **2026**, *6*, 49. [CrossRef]
24. Samadi, M.; Zirak, M.; Naseri, A.; Kheirabadi, M.; Ebrahimi, M.; Moshfegh, A.Z. Design and tailoring of one-dimensional ZnO nanomaterials for photocatalytic degradation of organic dyes: A review. *Res. Chem. Intermed.* **2019**, *45*, 2197–2254. [CrossRef]
25. Murali, R.; Amirthavalli, C. Defect assisted Reactive Oxygen Species generation for photocatalytic degradation of methylene blue by nano-structured zinc oxide synthesized in CTAB medium. *Mater. Chem. Phys.* **2023**, *294*, 127014. [CrossRef]
26. Chen, Y.; Wang, X.; Liu, B.; Zhang, Y.; Zhao, Y.; Wang, S. Directional regulation of reactive oxygen species in titanium dioxide boosting the photocatalytic degradation performance of azo dyes. *J. Colloid Interface Sci.* **2024**, *673*, 275–283. [CrossRef] [PubMed]
27. Ainali, N.M.; Kalaronis, D.; Evgenidou, E.; Bikiaris, D.N.; Lambropoulou, D.A. Insights into Biodegradable Polymer-Supported Titanium Dioxide Photocatalysts for Environmental Remediation. *Macromol* **2021**, *1*, 201–233. [CrossRef]
28. Capello, L.; Arsufi, A.B.L.; Lansarin, M.A. Self-Cleaning Films of Biopolymer Polyhydroxybutyrate with Different Semiconductors Incorporation: Development, Characterization, and Photocatalytic Activity Evaluation. *J. Appl. Polym. Sci.* **2024**, *141*, e56228. [CrossRef]
29. Shahmohammadi, M.; Nagay, B.E.; Barão, V.A.R.; Sukotjo, C.; Jursich, G.; Takoudis, C.G. Atomic Layer Deposition of TiO_2, ZrO_2 and TiO_2/ZrO_2 Mixed Oxide Nanofilms on PMMA for Enhanced Biomaterial Functionalization. *Appl. Surf. Sci.* **2022**, *578*, 151891. [CrossRef]
30. Liu, J.; Ma, X.; Yang, L.; Liu, X.; Han, A.; Lv, H.; Zhang, C.; Xu, S. In Situ Green Oxidation Synthesis of Ti^{3+} and N Self-Doped $SrTiO_x$ N_y Nanoparticles with Enhanced Photocatalytic Activity under Visible Light. *RSC Adv.* **2018**, *8*, 7142–7151. [CrossRef] [PubMed]
31. Hong, S.-G.; Hsu, H.-W.; Ye, M.-T. Thermal Properties and Applications of Low Molecular Weight Polyhydroxybutyrate. *J. Therm. Anal. Calorim.* **2013**, *111*, 1243–1250. [CrossRef]
32. Viana, M.M.; Soares, V.F.; Mohallem, N.D.S. Synthesis and Characterization of TiO_2 Nanoparticles. *Ceram. Int.* **2010**, *36*, 2047–2053. [CrossRef]
33. Socrates, G. *Infrared and Raman Characteristic Group Frequencies: Tables and Charts*, 3rd ed.; The University of West London: Middlesex, UK; J. Wiley and Sons: Chichester, UK, 2001; 348p.
34. Waweru, G.S.; Kiprotich, S.; Waithaka, P. Effects of Growth Temperature on the Structural and Optical Properties of Synthesized Titanium Dioxide Nanoparticles. *Am. J. Mater. Sci.* **2024**, *14*, 12–20.
35. Alothoum, M.A.S. A Review of the Synthesis, Structural, and Optical Properties of TiO_2 Nanoparticles: Current State of the Art and Potential Applications. *Crystals* **2025**, *15*, 944. [CrossRef]
36. Yurdakal, S.; Çetinkaya, S.; Augugliaro, V.; Palmisano, G.; Soria, J.; Sanz, J.; Torralvo, M.J.; Livraghi, S.; Giamello, E.; Garlisi, C. Alkaline Treatment as a Means to Boost the Activity of TiO_2 in Selective Photocatalytic Processes. *Catal. Sci. Technol.* **2020**, *10*, 5000–5012. [CrossRef]
37. Ali, H.; Nasr, R.A. Visible-Light-Driven ZnO/Y_2O_3@g-C_3N_4 Nanocomposite: Pioneering Ternary Photocatalyst for Efficient Water Purification. *Environ. Nanotechnol. Monit. Manag.* **2026**, *26*, 101163. [CrossRef]
38. Yasin, S.A.; Abbas, J.A.; Ali, M.M.; Saeed, I.A.; Ahmed, I.H. Methylene Blue Photocatalytic Degradation by TiO_2 Nanoparticles Supported on PET Nanofibres. *Mater. Today Proc.* **2020**, *20*, 482–487. [CrossRef]
39. Salah, Z.; Aloulou, H.; Bhattacharyya, S.; Cozzolino, V.; Algieri, C.; Chakraborty, S.; Calabrò, V.; Amar, R. Ben High-Performance Photocatalytic PSF/ZnO–GO Membranes for the Removal of Pharmaceuticals and Proteins from Wastewater. *Catal. Sci. Technol.* **2026**, *16*, 628–643. [CrossRef]
40. Negash, A.; Mohammed, S.; Weldekirstos, H.D.; Ambaye, A.D.; Gashu, M. Enhanced Photocatalytic Degradation of Methylene Blue Dye Using Eco-Friendly Synthesized rGO@ZnO Nanocomposites. *Sci. Rep.* **2023**, *13*, 22234. [CrossRef] [PubMed]
41. Kansal, S.K.; Kaur, N.; Singh, S. Photocatalytic Degradation of Two Commercial Reactive Dyes in Aqueous Phase Using Nanophotocatalysts. *Nanoscale Res. Lett.* **2009**, *4*, 709. [CrossRef] [PubMed]
42. Abu-Dalo, M.A.; Al-Rosan, S.A.; Albiss, B.A. Photocatalytic Degradation of Methylene Blue Using Polymeric Membranes Based on Cellulose Acetate Impregnated with ZnO Nanostructures. *Polymers* **2021**, *13*, 3451. [CrossRef] [PubMed]
43. Eswaran, P.; Madasamy, P.D.; Pillay, K.; Brink, H. Sunlight-Driven Photocatalytic Degradation of Methylene Blue Using ZnO/biochar Nanocomposite Derived from Banana Peels. *Biomass Convers. Biorefinery* **2025**, *15*, 12347–12367. [CrossRef]
44. Paredes, P.; Rauwel, E.; Wragg, D.S.; Rapenne, L.; Estephan, E.; Volobujeva, O.; Rauwel, P. Sunlight-Driven Photocatalytic Degradation of Methylene Blue with Facile One-Step Synthesized Cu-Cu_2O-Cu_3N Nanoparticle Mixtures. *Nanomaterials* **2023**, *13*, 1311. [CrossRef] [PubMed]
45. Vavilapalli, D.S.; Peri, R.G.; Sharma, R.K.; Goutam, U.K.; Muthuraaman, B.; Ramachandra Rao, M.S.; Singh, S. G-C_3N_4/$Ca_2Fe_2O_5$ Heterostructures for Enhanced Photocatalytic Degradation of Organic Effluents under Sunlight. *Sci. Rep.* **2021**, *11*, 19639. [CrossRef] [PubMed]

46. Avilés-Monreal, R.; Cárdenas-Rodríguez, A.; Farías, M.H.; Borbón-Nuñez, H.A.; Castillón-Barraza, F. Degradation of Methylene Blue Catalyzed by a Photo-Fenton Reaction of G-C_3N_4/Fe_3O_4 Nanocomposite with Visible Light. *Fuller. Nanotub. Carbon Nanostructures* **2026**, *34*, 277–290. [CrossRef]
47. Upadhaya, D.; Kumar, P.; Dhar Purkayastha, D. Superhydrophobic ZnO/TiO_2 Heterostructure with Significantly Enhanced Photocatalytic Activity. *J. Mater. Sci. Mater. Electron.* **2019**, *30*, 10399–10407. [CrossRef]
48. Diaz-Uribe, C.; Duran, F.; Vallejo, W.; Puello, E.; Zarate, X.; Schott, E. Photocatalytic Study of TiO_2 Thin Films Modified with Anderson-Type Polyoxometalates (Cr, Co and Ni): Experimental and DFT Study. *Polyhedron* **2023**, *231*, 116253. [CrossRef]
49. Wongrerkdee, S.; Wongrerkdee, S.; Boonruang, C.; Sujinnapram, S. Enhanced Photocatalytic Degradation of Methylene Blue Using Ti-Doped ZnO Nanoparticles Synthesized by Rapid Combustion. *Toxics* **2023**, *11*, 33. [CrossRef] [PubMed]

Disclaimer/Publisher's Note: The statements, opinions and data contained in all publications are solely those of the individual author(s) and contributor(s) and not of MDPI and/or the editor(s). MDPI and/or the editor(s) disclaim responsibility for any injury to people or property resulting from any ideas, methods, instructions or products referred to in the content.